Published in final edited form as:
Toxicol Lett. 2013 June 20; 220(1): 44–52. doi:10.1016/j.toxlet.2013.04.003.

Microglial disruption in young mice with early chronic lead exposure☆

Christina Sobin[a,b,c,d,*], **Mayra Gisel Flores Montoya**[c], **Natali Parisi**[e], **Tanner Schaub**[e], **Miguel Cervantes**[a], and **Rodrigo X. Armijos**[a]

[a]Department of Public Health Sciences, College of Health Sciences, University of Texas, El Paso, USA

[b]Border Biomedical Research Center, College of Science, University of Texas, El Paso, USA

[c]Department of Psychology, University of Texas, El Paso, USA

[d]Laboratory of Neuroendocrinology, The Rockefeller University, New York, NY, USA

[e]Laboratory of Chemical Analysis and Instrumentation, New Mexico State University, Las Cruces, NM, USA

Abstract

The mechanisms by which early chronic lead (Pb) exposure alter brain development have not been identified. We examined neuroimmune system effects in C57BL/6J mice with Pb exposure, including levels that may be common among children in lower socioeconomic income environments. Pups were exposed via dams' drinking water from birth to post-natal day 28 to low, high or no Pb conditions. We compared gene expression of neuroinflammatory markers (study 1); and microglial mean cell body volume and mean cell body number in dentate gyrus, and dentate gyrus volume (study 2). Blood Pb levels in exposed animals at sacrifice (post-natal day 28) ranged from 2.66 to 20.31 μg/dL. Only interleukin-6 (IL6) differed between groups and reductions were dose-dependent. Microglia cell body number also differed between groups and reductions were dose-dependent. As compared with controls, microglia cell body volume was greater but highly variable in only low-dose animals; dentate gyri volumes in low- and high-dose animals were reduced. The results did not support a model of increased neuroinflammation. Instead, early chronic exposure to Pb disrupted microglia via damage to, loss of, or lack of proliferation of microglia in the developing brains of Pb-exposed animals.

Keywords

Pb; Microglia; Neuroinflammation; Neurotoxicity; Dentate gyrus

1. Introduction

In children with no observable peripheral symptoms of Pb exposure ("asymptomatic"), blood Pb levels as low as 2.5 μg/dL have been associated with, for example, lower IQ,

*Corresponding author at: Department of Public Health Sciences, College of Health Sciences, University of Texas, El Paso, USA. Tel.: +1 9157478485; fax: +1 9157476553. casobin@utep.edu (C. Sobin).

Conflict of interest statement The authors declare that there are no conflicts of interest.

reduced academic achievement, and poorer memory, attention, motor dexterity and problem-solving, suggestive of altered brain development (Canfield et al., 2003; Chiodo et al., 2004; Lanphear et al., 2005). In mouse and rodent models, early chronic exposure to Pb resulted in decreased memory, and abnormal motor and exploratory behavior (Azzaoui et al., 2009; Kasten-Jolly et al., 2012; Leasure et al., 2008). The mechanisms by which early chronic exposure to Pb alters brain structure and function have not been identified.

Results from in vivo and in vitro studies have suggested that Pb may promote neurotoxicity by disrupting neuroimmune system function (Kraft and Harry, 2011). The neuroimmune system is comprised of microglial cells. Microglia protect brain tissue through constant surveillance and scavenging of debris and foreign substances from the local environment (Schwartz et al., 2006); microglia also facilitate neuronal activity, and interact functionally with astrocytes (Aloisi, 2001). During development, activated microglia support and protect neurite development, guide synaptic pruning, and sculpt neural circuits (Paolicelli et al., 2011; Ransohoff and Cardona, 2010; Schafer et al., 2012). The critical neuroprotective role of microglia during early development is suggested by the acute sensitivity of these cells to CNS changes, as indicated by extremely rapid activation and proliferation response times (Dissing-Olesen et al., 2007). Microglia express IBA-1 thus IBA-1 antibody is used in immunohistochemical preparations to label microglia in brain tissue.

Microglia are activated by various agents that trigger a sequence of unique morphologic changes, including cell body enlargement. Activated microglia secrete an array of chemokines, eicosanoids, proteases, complements, and cytokines including, for example, TNF-α, IL-1β, IL-6, IL-10, and IFN-γ. The influence of a given cytokine is not singular, and at different times, might be pro- or anti-inflammatory, and thus have neuro-protective or neuro-destructive effects. Free radicals are increased by up-regulation of iNOS; and astrocytes simultaneously induce HO-1 which promotes reduction of damaging ROS (Min et al., 2006). During activation, microglia proliferate, and proliferation is stimulated by IL1-β and TNF-α (Mander et al., 2006). If microglial activation becomes chronic, microglia synthesize neurotoxic levels of quinolinic acid (Espey et al., 1997) and promote extracellular glutamate concentrations sufficient to cause neuritic beading and cell death (Takeuchi et al., 2005). Pro-inflammatory cytokines inhibit glutamate transporters, which sustain abnormally high levels of extra-cellular glutamate and thus, cyclic re-activation (Minami et al., 1991).

Findings from in vivo and in vitro studies show that Pb exposure alters cellular functions in ways that might be expected to promote chronic microglial activation. Pb accumulation in erythrocytes results in increased brain δ-ALA which enhances and prolongs microglial activation (Kaushal et al., 2007). Moreover, microglia interact functionally with astrocytes, via cytokines (Verderio and Matteoli, 2001), prostaglandins (Mohri et al., 2006) and nitric oxide synthase (Sola et al., 2002). Excess δ-ALA irreversibly inhibits glutamate uptake by astrocytes, via alteration of the glutamate transporter GLT-1 (Emanuelli et al., 2003). Glutamate potentiates astrocytic increases in Ca^{2+} via activation of metabotropic glutamate receptors (Zonta et al., 2003). δ-ALA triggers astrocytic Ca^{2+} waves which in turn activate microglia over large distances (Schipke et al., 2001).

Thus, by way of multiple mechanisms, free-floating Pb in brain tissue and increased brain δ-ALA might be expected to promote neuroimmune system disruption, chronic microglial activation and microglia proliferation, as evidenced by altered levels of pro- and anti-inflammatory markers including TNF-α, IFN-γ, IL6, IL10, iNOS and HO-1, increased microglial mean cell body number, and mean cell body volume.

The aim of this study was to examine evidence of neuroimmune and brain structure differences in young C57BL/6J mice, with and without chronic Pb exposure. In child

studies, Pb exposure has been associated with reduced short-term and working memory (see Section 1), which are subserved by dentate gyrus (DG) (Niewoehner et al., 2007), a sub-component of the hippocampal formation. In rodent models, low-level Pb exposure resulted in diminished recognition memory (see Section 1) which is also subserved by dentate gyrus (Jessberger et al., 2009); moreover, DG microglia have been shown to play a critical role in the maintenance of neural genesis and spatial learning and memory (Ziv et al., 2006).

In animals with and without Pb exposure, we compared gene expression levels of neuroinflammatory markers (TNF-α, IFN-γ, IL6, IL10, HO-1, iNOS, and GRP78) in anterior (without hippocampus/DG) and posterior (with hippocampus/DG) brain regions. In a separate study, in animals with and without Pb exposure, we measured IBA-1 labeled microglia mean cell body number and mean cell body volume; and volume of DG. We predicted significant dose-dependent group differences on outcome measures. Only IL6 differed between groups and reductions were dose-dependent. Microglia mean cell body number also differed between groups and reductions were dose-dependent. Microglia mean cell body size differed only among low-dose animals. As compared with controls, dentate gyrus volumes in Pb-exposed animals were reduced.

2. Materials and methods

2.1. Animal methods

This study was carried out in strict accordance with the recommendations in the Guide for the Care and Use of Laboratory Animals of the National Institutes of Health. The protocol was approved and annually reviewed by the Institutional Animal Care and Use Committee of the University of Texas at El Paso (NIH Assurance #A3340-01). All surgery was performed under deep Avertin anesthesia and all efforts were made to minimize suffering. C57BL/6J (Jax Mice, Jackson Laboratory, Sacramento, CA) mice were bred and housed at the University of Texas at El Paso Biosciences Research Facility, Animal Vivarium, in clear polycarbonate cages with wood chip bedding, 1 litter per container. Animals were maintained on a 12 h light–dark schedule, vivarium temperature of 21 ± 2 °C, with ad libitum access to food and water. Dams' drinking water was tainted with 99.4% Pb acetate crystals (Sigma–Aldrich). To maximally reduce animal stress, no invasive procedures were conducted during the 28-day exposure period, litters were not culled, and studies included males and females. Natural litters were exposed from birth to one of three possible Pb doses: 0 ppm; 30 ppm; and 230 ppm (study 1) or 0 ppm; 30 ppm; and 330 ppm (study 2). For both studies, the dosing regimen was based on pilot studies demonstrating that 30–40 ppm of Pb acetate in dams' drinking water resulted in a blood Pb level range similar to at least 65% of low-income children tested in our child Pb exposure and behavior studies (unpublished data).

2.2. ICP-MS analysis of Pb

2.2.1. Instrumentation—Analysis by inductively coupled plasma mass spectrometry (ICP-MS) was performed with an Agilent 7500ce ICP/MS equipped with an octopole reaction system and a CETAC ASX-520 autosampler as previously described (Sobin et al., 2011). Briefly, samples were introduced to the plasma through a MicroMist U-series nebulizer (Glass Expansion, Australia) and a double-pass quartz spray chamber (Agilent, Santa Clara, CA). Instrument parameters were: carrier gas, 0.78 L/min; makeup gas, 0.15 L/min; RF power, 1420 W; spray chamber temperature, 2 °C.

2.2.2. Sample treatment and analysis—Certified whole blood standards (Le Centre de Toxicologie du Quebec) were analyzed to determine instrument reproducibility and validate quantitation. Ten solutions were prepared for each of two standards (4.00 μg/dL and 6.59

μg/dL) and each of those were analyzed three times by ICP-MS. Standard concentrations were chosen to approximate low blood Pb values of children in this study. Blood standards were prepared as previously described (Sobin et al., 2011) (Agilent technical note #5988-0533EN). Briefly, 5.58 mL of water (18 MΩ DI, Labconco WaterPro® PS Station, Kansas City, MO) was placed in a polypropylene tube into which 300 μL of whole blood was added, followed by addition of by 60 μL of aqueous internal standard solution (100 ppb each germanium, yttrium and terbium in 5% nitric acid, Fisher Optima) and 60 μL of aqueous 10 ppm gold in 3% hydrochloric acid (EMD Chemicals) solution. The final dilution was twenty-fold, the final internal standard concentration was 1 ppb and the final gold concentration was 100 ppb. A six-point external calibration curve was prepared from a Pb stock solution in 1% nitric acid. ICP-MS standard solutions containing the elements in 2% nitric acid were obtained from Inorganic Ventures (Christiansburg, VA). Samples were vortexed for a few seconds prior to a 1 min centrifugation at 2000 rcf and the supernatant analyzed by ICP-MS. Blank solutions were analyzed after every three samples throughout the analytical sequence and standard check solutions were analyzed five times, interspersed through the sequence. All samples produced signals in excess of the limit of quantitation (i.e. ten-fold greater than the detection limit) for each analyte.

2.3. Gene expression studies

Brain tissue was removed immediately after sacrifice, snap frozen on dry ice and stored at −80 °C until RNA extraction. Cerebellum was removed and the remaining whole brain structure was cut (within 1 min) into anterior and posterior sections; and sections were immediately homogenized (30 s). Anterior segments included at least 90% of basal forebrain, striatum, ventral striatum and septum; and no more than 10% of hippocampus, amygdala, thalamus, and hypothalamus. Posterior sections included at least 90% of the midbrain, hippocampus, amygdala, thalamus, and hypothalamus; and no more than 10% of basal forebrain, ventral striatum, septum, and striatum.

2.3.1. RNA extraction—RNA was extracted using RiboPure™ Kit (Ambion). All procedures were conducted at room temperature unless otherwise specified. Each section was homogenized individually with 400 μL of TRI Reagent®. After homogenization, 100 μL of chloroform was added, the mixture was vortexed (15 s), incubated (5 min), and centrifuged at 12,000 × *g* (10 min). The aqueous layer was transferred to a micro-centrifuge tube with 100 μL of 100% ethanol, vortexed (5 s) and transferred to a (kit-supplied) filter cartridge and collection tube. The filter and collection tube were centrifuged at 12,000 × *g* (1 min) to accomplish binding of the RNA to the filter. After discarding the flow-through liquid, the filter was replaced and 250 μL wash solution was added to the tube was and centrifuged at 12,000 × *g* (1 min), and repeated. With the filter was in a new tube, 40 μL of Elution Buffer was added to recover the RNA and incubated (2 min). After incubation, the tube was centrifuged at 12,000 × *g* (90 s). DNase was added to digest any remaining DNA. To each RNA sample, 1 μL of 10× DNase I Reaction Buffer and 1 μL of DNase I Amplification grade was added and incubated (15 min). After incubation, 1 μL of 25 mM EDTA solution was added and the mixture heated to 65 °C (10 min). After treatment with DNase, RNA concentration was obtained using an ND-1000 (NanoDrop Technologies). RNA integrity was determined by 1.2% agarose gel. The RNA purity was assessed by spectrometry (260/280 ratios).

2.3.2. cDNA synthesis—cDNA synthesis was conducted immediately after RNA extraction to reduce RNA degradation using High Capacity cDNA Reverse Transcription Kit (Applied Biosystems). Ten μL of prepared master mix was combined with 10 μL of extracted RNA in a 0.2 mL tube, centrifuged briefly, and loaded into a GeneAmp® PCR

System 9700 thermal cycler (Applied Biosystems). Tubes containing cDNA were stored at −80 °C until gene expression analysis.

2.3.3. Gene expression analysis—Gene expression was determined with quantitative real-time polymerase chain reaction (QRT-PCR) and mRNA TaqMan® gene probes were used to quantitate expression of TNF-μ, INF-μ, IL-6, IL-10, iNOS, HO-1, and GRP78. The "housekeeping" gene beta-actin was used as the endogenous control for normalization of the biomarker RNA quantities. A 96-well QRT-PCR plate was prepared containing an amount of cDNA equivalent to 500 ng of RNA, 1 μL TaqMan® probe, 10 μL TaqMan® Universal Master Mix, and an amount of nuclease free water that brought the total volume in each well to 20 μL. Filled plates were placed in an iCycler iQ™ Optical Module thermal cycler (BIO RAD) and the levels of each biomarker were measured. All reactions were run in triplicate.

2.3.4. Statistical analysis for gene expression studies—SAS version 9.1 software was used for all analyses. Data were entered and checked for accuracy and distribution properties prior to analysis. Normalized expression ratios were determined using the $2^{-\Delta\Delta C_T}$ (Livak) method (Livak and Schmittgen, 2001). Mean ratios of expression ("fold-change") for each biomarker were compared using a 3 (group) × 2 (sex) × 2 (anterior/posterior section) general linear model ANOVA. Type III sum of squares were used to determine statistically significant differences; post hoc tests of marginal means ("least square means") were conducted for all significant ANOVA models. When significant group effects were found, linear regression analyses were used to test for dose–response relationships.

2.4. Immunohistochemistry

Mice were anesthetized with Avertin (Gaertner et al., 2008) immediately prior to sacrifice and perfused transcardially with 10% sucrose followed by phosphate-buffered 4% paraformaldehyde. (A sucrose rather than saline pre-wash was used to reduce cell distortion.) After removal, brains were post-fixed in the same fixative overnight at 4 °C. Whole brains were randomly selected from each group for immunohistochemical studies and included 10 controls, 10 low-dose, and 10 high-dose brains. After cryoprotection in 0.1 M phosphate buffer (pH 7.4) containing 20% sucrose for up to 72 h (until sinking) at 4 °C, brains were rapidly frozen in isopentane pre-cooled to −75 °C with dry ice. All frozen brains were stored at −75 °C before sectioning. Serial cryostat sections were cut in a systematic–random manner at an instrument setting of 40 μm in the coronal plane through the whole brain, including the brain stem and the cerebellum (Franklin and Paxinos, 1997). Four adjacent sets of four sections were collected into separate wells for staining, generating approximately 70 sections per set.

All sections of the first set were processed for IBA-1 immunostaining with commercially available specific antibodies (given below). After inactivating the endogenous peroxidase activity with hydrogen peroxidase, sections were incubated separately with avidin and biotin solutions (Vector Lab, Burlingame, CA) to block nonspecific binding of endogenous biotin. Sections were then incubated free-floating for 43 h at 4 °C in 0.01 M phosphate-buffered saline (PBS, pH 7.4) containing 1% normal donkey serum, 0.3% Triton X-100 (Sigma, St. Louis, MO) and rabbit anti-Iba-1 IgG (1:6000, Cat.# 019-19741, Wako Chemicals USA, Richmond, VA). Subsequently, the immune-reaction product was visualized using the avidin–biotin complex method of Hsu et al. (1981). In brief, sections were incubated in PBS containing normal donkey serum, Triton-X and biotin-SP-AffiniPure donkey anti-rabbit IgG (Jackson ImmunoResearch Labs, West Grove, PA) for 1 h, and then in PBS containing avidin-biotinylated horseradish peroxidase complex (Vectastin elite ABC kit, Vector Lab) for another hour. This was followed by incubation of the sections for 5 min in 0.05 M Tris buffer (pH 7.2) containing 0.03% 3′,3′-diaminobenzidine (Sigma) and 0.0075% H_2O_2. All

steps were carried out at room temperature except where indicated, and each step was followed by washes in PBS. After thorough washes, all sections were mounted on gelatin-coated slides, and then were counterstained with FD cresyl violet solution™ (FD NeuroTechnologies). Following dehydration in ethanol and clearing in xylene, sections were coverslipped with Permount® (Fisher Scientific, Fair Lawn, NJ).

2.5. Stereology

2.5.1. Anatomy—The upper and lower blades of the dentate gyrus (DG) contain three distinct layers (molecular, granule and polymorphic). The C57BL/6 mouse DG extends from coronal levels 64–93. The boundaries of the DG were defined according to the Allen Reference Atlas for the C57BL/6J mouse brain (Dong, 2008). This reference atlas was used throughout data collection, and was consulted prior to DG demarcation of each section.

2.5.2. Procedures—Prior to beginning data collection, for each subject, the total number of sections through the DG was determined. A pilot study of two animals (one from the 330 ppm exposure group and one from the control group) was conducted to determine an optimal sampling scheme that would result in estimates of the coefficient of error (CE) at or below 0.15 while ensuring sampling efficiency. A high stringency sampling approach was used in which sampling continued until the mean CEs for all outcome variables were <0.15 (Table 2) (Gundersen et al., 1999).

The estimation of DG microglia mean body cell volume, microglia mean body cell number, and DG volume, was assisted by *Stereologer*™ software (Stereology Resource Center, Chester, MD). The software was installed on a Dell Optiplex tower computer and connected to a Nikon Eclipse E600 microscope (Nikon, Melville, NY) fitted with an *X*–*Y*–*Z* motorized stage controller (Prior Scientific, Rockland, MA), linear encoder microcator (*z*-axis gauge) (Heidenhain, Schaumburg, IL), high resolution color video camera (IMI Tech, Inc., Encinitas, CA) and .50 C-mount (Nikon, Melville, NY). DG volume was estimated at 4× (Nikon Plan 4× 0.10); DG microglia mean cell volume and mean cell number were estimated at 60× (Nikon Plan APO 1.40 Oil). The camera image was processed with a high resolution video card and displayed on a 21 in. high resolution Dell monitor. One experimenter (C.S.) collected all of the stereological data without knowledge of the blood Pb level of each subject; the experimenter was not blind to treatment group.

2.5.2.1. Dentate gyrus microglia mean cell number: An unbiased estimate of the number of microglia in the DG was obtained using the optical fractionator method (West et al., 1991) as reported previously for quantification of total number of microglia in mouse models of aging and neuropathology (Mouton et al., 2002). For each section the software randomly sampled virtual 3-D counting frames (disector) at 60× magnification with a 2 μm guard area. Using thin-focal plane optical scanning, microglia were counted when they fell within the central depth of the counting frame and/or touched the inclusion lines. The total number of microglia was estimated with the following formula: $N_{obj} = \Sigma Q^{-} \times 1/\text{SSF} \times 1/\text{ASF} \times 1/\text{TSF}$; where ΣQ^{-} = sum of the objects sampled; SSF = sampling interval; ASF = total area sampled/total area on all sampled sections; and TSF = the height of the sample/total section thickness.

2.5.2.2. Dentate gyrus mean cell volume: For each frame, mean cell volume was quantified on microglia counted with the disector probe.

2.5.2.3. Dentate gyrus volume: The dentate gyrus reference volume ($V_{(\text{ref})}$) was determined at 4× magnification using the Cavalieri-point counting approach (Gundersen and Jensen, 1987): $V_{(\text{ref})} = ([k \times t] \times \Sigma P \times [a(p)M^2])$; where: k = sampling interval; t = post-processing

section average thickness; and thus [$k \times t$] = distance between planes; ΣP= sum of points counted; [$a(p)/M^2$] = test grid area per point (μm^2) divided by the magnification factor squared. Examples of microglia images are provided in Fig. 4.

2.5.2.4. Statistical analysis of stereological results: *SAS Version 9.2* statistical software was used for all analyses. All data were entered and checked for accuracy and distribution properties prior to analysis. No extreme outliers were identified, and all data were included for analysis. Coefficient of error values and section thickness, and DG microglia mean cell volume, DG microglia mean cell number, and DG volume were compared using a 3 (group) × 2 (sex) general linear model ANOVA. Type III sum of squares were used to determine statistically significant differences; post hoc tests of marginal means ("least square means") were conducted for all significant ANOVA models. When significant group effects were found, linear regression analyses were used to test the possible dose–response relationship between blood Pb level and the outcome variable.

3. Results

3.1. Neuroinflammatory markers (study 1)

We analyzed blood samples and brain tissue from N = 16 (10 male) C57BL/6J mice exposed from birth to PND 28, to one of three Pb exposure treatments via dams' drinking water: 30 ppm, n = 6 (4 males); 230 ppm, n = 4 (2 males); 0 ppm, n = 6 (3 males). The mean (SD) blood Pb levels of mice at sacrifice (PND 28) were: controls = 0.22 μg/dL (0.13); 30 ppm = 4.12 μg/dL (1.49); 230 ppm = 10.31 μg/dL (2.42). Gene expression levels were determined with real-time quantitative-polymerase chain reaction (QRT-PCR). The $2^{-\Delta\Delta C_T}$ (Livak) method (Livak and Schmittgen, 2001) was used to quantify differences in gene expression relative to the external control. The fold-change for each probe was compared using 3 (group) × 2 (sex) × 2 (anterior/posterior section) ANOVA; significant models were further tested with post hoc tests of marginal means ("least square means"). The amplification ratios for biomarkers and beta-actin were 0.95–0.97.

The relative quantification values in fold-change for each biomarker are given for anterior brain and posterior brain (Table 1). ANOVA analyses revealed significant group differences only for IL6, model $F_{11,19} = 3.52$, $p < 0.01$; type III SS for group main effect, $F = 6.48$, $p < 0.01$; and for anterior/posterior main effect, $F = 13.82$, $p < 0.01$; no main effect for sex; no significant interactions.

Tukey's post hoc analyses revealed significant differences ($p < 0.01$) between controls and 30 ppm group (1.93 + 0.14 vs. 1.29 + 0.18); and between controls and 230 ppm group (1.93 + 0.14 vs. 1.17 + 0.17); and no significant difference in IL6 expression between 30 ppm and 230 ppm groups.

Tukey's post hoc analyses confirmed a significant difference, $t = 4.12$, $p < 0.01$, between IL6 expression in anterior vs. posterior brain (1.74 + 0.13 vs. 1.18 + 0.13). Regression analyses predicting IL6 fold-change from blood Pb level were significant, suggesting a small dose–response effect. In posterior brain, as blood Pb level increased, IL6 decreased, $adj\ r^2$ = 0.21; IL6 = 1.52 + (−0.06 × blood Pb level). A small significant association was also observed in anterior brain, $adj\ r^2$ = 0.24; IL6 = 2.23 + (−0.08 × blood Pb).

3.2. Stereological analysis of microglia and dentate gyrus volume (study 2)

Mean cell body volume, mean cell body number and dentate gyrus volume was quantified in brain tissue from N = 30 (17 males) C57BL/6J mice exposed from birth to PND 28, to one of three Pb exposure treatments via dams' drinking water: 30 ppm, n = 10 (6 males); 330 ppm, n = 10 (4 males); or 0 ppm, n = 10 (7 males). The mean (SD) blood Pb levels of mice

at sacrifice (PND 28) were 30 ppm = 3.42 μg/dL (0.71); 330 ppm = 13.84 μg/dL (2.86); controls = 0.03 μg/dL (0.01). Coefficient of error estimates for the measurement of dependent variables are shown in Table 3. The distributions of group means, standard deviations, minimum and maximum values for microglia mean cell body volume, microglia mean cell body number, and volume of DG are shown in Figs. 1–3.

3.2.1. Microglia mean cell body volume—Two-way ANOVA (group × sex) indicated a statistically significant difference among the groups ($F_{2,27} = 12.01$; $p < 0.01$; Table 1) with no main effect for sex; and no interaction.

Further analysis with Tukey's post hoc tests revealed that, as compared with controls (114.39 + 20.62; 95% C.L. 96.57–132.21), microglia mean cell body volume of the 30 ppm Pb exposure group was significantly larger (154.92 + 40.35; 95% C.L. 137.10–172.74), $t = 3.30$, $p < 0.01$. As compared with controls, the microglia mean cell body volume of the 330 ppm Pb exposure group (96.09 + 14.49; 95% C.L. 78.27–113.91) did not differ significantly, $t = 1.49$, $p = 0.15$, and thus a dose–response effect was not observed.

3.2.2. Microglia mean cell body number—Two-way ANOVA (group × sex) indicated a statistically significant difference among the groups ($F_{2,27} = 24.49$; $p < 0.01$; Table 1) with no main effect for sex; and no interaction.

Tukey's post hoc tests revealed that, as compared with controls (7116 + 1363; 95% C.L. 6501–7730), the microglia mean cell body number of the 30 ppm Pb exposure group was significantly decreased (5274 + 808; 95% C.L 4660–5889), $t = -4.35$, $p < 0.01$. Similarly, as compared with controls, the microglia mean cell body number of the 330 ppm Pb exposure group was significantly decreased (4184 + 423; C.L. 3569–4789), $t = -6.92$, $p < 0.01$. Microglia mean cell body number of the 30 ppm and 330 Pb exposure group differed significantly, $t = -2.57$, $p = 0.02$, suggesting a dose response relationship between DG microglia number and blood Pb level.

Thus, from 30 animals, we attempted to predict DG microglia mean cell body number from blood Pb levels using simple linear regression analysis. A moderate linear association was suggested. The slope of the regression line was significantly less than zero, suggesting that as blood Pb level increased, the number of DG microglia decreased (slope = −170; 95% C.L. −240 to −101; $t_{28} = -5.02$; $p < 0.01$; DG microglia = 6505 + (−170 × blood Pb level); $adj\ r^2 = 0.47$).

3.2.3. Dentate gyrus volume—Two-way ANOVA (group × sex) indicated a statistically significant difference among the groups ($F_{2,27} = 11.50$; $p < 0.01$; Table 1); with no main effect for sex, and no interaction.

Tukey's post hoc tests revealed that, as compared with controls (0.38 mm^3 + 0.06; 95% C.L. 0.35–0.41), the DG volume means of the 30 ppm Pb exposure group (0.29 mm^3 + 0.03; 95% C.L 0.26–0.32), ($t = -4.65$, $p < 0.01$); and the 330 ppm Pb exposure group (0.31 mm^3 + 0.04; C.L. 0.28–0.34), ($t = -3.35$, $p < 0.01$); were significantly decreased. DG volumes of the 30 ppm and 330 ppm Pb exposure groups were not statistically significant ($t = -1.30$, $p = 0.20$) suggesting that the relationship between blood Pb level and DG volume was not linear.

To examine whether the microglial cell loss might account for reduced DG volume, from 30 animals, we attempted to predict DG volume from microglial cell body number using simple linear regression analysis. A small linear association was suggested. The slope of the regression line was significantly greater than zero, suggesting that as microglial cell body

number increased, DG volume increased (slope = 0.000019 mm^3; 95% C.L. 0.00000564–0.00003169 mm^3; $t_{28} = 6.12$; $p < 0.01$; $Y = 0.22\ mm^3 + (0.00019\ mm^3 \times X)$; $adj\ r^2 = 0.20$).

4. Discussion

4.1. Overview

Previous research suggested that via diverse mechanisms Pb exposure promotes neuroimmune disruption, and perhaps chronic microglial activation and microglial proliferation (Kraft and Harry, 2011). Neuroimmune system changes following early chronic exposure to Pb and blood levels between 2 μg/dL and 20 μg/dL have rarely been examined. Hippocampus/DG regions have been implicated in animal models (Azzaoui et al., 2009; Kasten-Jolly et al., 2012; Leasure et al., 2008) and clinical studies of asymptomatic Pb exposed children (Canfield et al., 2003; Chiodo et al., 2004; Lanphear et al., 2005). Thus, we compared neuroinflammatory markers in anterior (without hippocampus) and posterior (with hippocampus) brain sections; and we compared the volume and number of neuroimmune cells in the DG. We predicted dose-dependent changes in gene expression of neuroinflammatory biomarkers consistent with heightened microglial activation, and increased microglial mean cell body volume and number. Understanding whether dose–response relationships exist between Pb and outcome variables can be critical for understanding the nature of possible mechanisms of action, and also for comparison in subsequent studies that aim to replicate and refine the current findings. We also measured DG volume to examine evidence of neurodegeneration. The range of blood Pb levels achieved in the 30 ppm exposure groups (study 1 = 2.86–6.78 μg/dL; study 2 = 2.48–4.65 μg/dL) replicated the blood Pb levels of approximately 65% of low-income children tested in our child Pb exposure studies (unpublished data). Significant differences between exposure groups on outcome variables were found, but were not suggestive of heightened microglial activation.

4.2. No evidence for increased neuroinflammation in Pb exposed animals

Increased neuroinflammatory response in Pb exposed animals was discounted by the absence of group effects for five of six neuroinflammatory markers examined, including TNF-α, IFN-γ, IL10, iNOS and HO-1. Only IL6 differed in Pb exposed animals, and a dose-dependent reduction was observed. Astrocytes absorb free-floating brain Pb; within astrocytes 78 kDa glucose-regulated protein (GRP78) sequesters Pb, a process which inactivates this chaperone protein (Lindahl et al., 1999) and results in decreased release of IL6 (White et al., 2007). IL6 serves neuroprotective and neuroadaptive functions (Gruol et al., 2011; Inomata et al., 2003) thus reduced IL6 may suggest one source of increased neurotoxic vulnerability in Pb exposed animals. Reduction of astrocytic IL6 release reduces functional coupling of microglia and astrocytes, and disrupts regulation of microglia by astrocytes (Hinkerohe et al., 2005). Reduction of IL6, with no changes observed in TNF-α, IFN-γ, IL10, iNOS and HO-1, suggested that IL6 differences were not linked to heightened neuroinflammation.

4.3. Broad variability of microglial volume in low-exposure animals

Microglia mean cell body volume of animals from the 30 ppm group with blood Pb levels between 2.48 μg/dL and 4.65 μg/dL exceeded that of the controls by 40.53 μm^3, however the larger group mean was derived from an extremely broad range of cell sizes in the low-dose animals (Fig. 1) that was unique to the low-dose animals. Morphological studies of qualitative cell features are needed to examine structural sources of these observed volumetric differences. (Microglia mean cell body volume of the 330 ppm animals did not differ significantly from controls. This will be discussed further below.)

4.4. Reduced numbers of detectable microglia in low- and higher-exposure animals

During activation microglia proliferate. With regard to DG microglia number, counter to our hypothesis, as compared with controls the microglia mean cell body number of the 30 ppm exposure group was significantly decreased (1842 fewer cells). In the 330 ppm exposure group, as compared with controls, the decrease was even greater (2932 fewer cells), and differed significantly from the 30 ppm exposure group. Regression analysis confirmed that the effects were dose-dependent and suggested that for each one unit (μg/dL) increase in blood Pb, DG microglia decreased by 170 cells.

There are several possible sources of fewer detectable IBA-1 labeled microglia in Pb-exposed animals. IBA-1 is present in all normal microglia and it is up-regulated during activation. IBA-1 critically regulates membrane ruffling, cell motility and phagocytosis (Deininger et al., 2002; Ito et al., 1998). Fewer detected IBA-1 labeled microglia in Pb exposed animals could result from disrupted production of IBA-1 in microglia (which in turn would disable normal microglial cell function). Determining whether the findings reflect fewer normally functioning microglia, rather than reduction of total microglial cells, requires further study. Also of note, whether IBA-1 is expressed exclusively by microglia has been recently questioned. For example, one study of rat brain suggested that other types of macrophages also express IBA-1 including meningeal, supra ependymal, and vascular stromal cells (Kirik et al., 2011). Of these, stromal cells may be found in dentate gyrus, and their morphology differs from that of microglia. This is a consideration for future studies of neuroimmune function and Pb exposure that examine brain regions likely to include these types of macrophages.

Another explanation concerns proliferation mechanisms. Studies have suggested that the P2X7 receptor is critical for microglial proliferation during activation (Monif et al., 2010). Future studies could examine the effects of brain Pb and/or increased δ-ALA on P2X7 and thus proliferation.

The effects of Pb on microglia progenitors also should be considered. Microglia are derived from hematopoietic stem cells in bone marrow. Some of these stem cells differentiate as monocytes and further differentiate as microglia in the brain (Ritter et al., 2006). Pb is sequestered in bone marrow. Studies are needed to examine whether Pb in bone marrow disrupts critical replenishment of the hematopoietic daughter cell pool, thus reducing the migration of adequate progenitor cell numbers to the brain.

Finally, reduced numbers of IBA-1 labeled microglia may suggest that early chronic Pb exposure resulted in direct destruction of microglia. Astrocytes are typically noted to be the brain's "lead-sink." The primary role of microglia however is to scavenge the brain for debris; further studies are needed to examine whether microglia are destroyed by scavenged Pb particles.

Very recent studies have illuminated the critical role of microglia in brain development (Paolicelli et al., 2011). Additional studies are needed to examine whether pruning abnormalities are evident in mice with early chronic Pb exposure, and whether reduced numbers of functional microglia in lead exposed animals compromises the neuroimmune response system.

4.5. Reduced volume of dentate gyri in Pb-exposed animals

Given the potential neurodegenerative effects of disrupted neuroimmune function, we also examined DG volume. As compared with controls, DG volume in both exposure groups was significantly decreased, and exposure groups did not differ significantly. Because both exposure groups received chronic dosing, the lack of difference between low and higher

exposure groups with regard to DG volume suggested that the chronicity of exposure may have had more neuropathological significance than the amount of Pb to which the mice were exposed. Studies are needed to compare DG volume differences in cases of chronic versus acute exposure, to test how chronicity of exposure influences the effects of early chronic Pb exposure on brain structure volume.

Reduced DG volume could suggest either developmental delay of structure volume, or tissue deterioration in Pb-exposed animals. The lack of difference between low and higher Pb exposure groups suggested that whatever qualitative differences may exist between early chronic Pb exposure levels, delay and/or deteriorative effects on development of dentate gyrus volume are not distinguishable in animals with low and higher exposures. We also examined the association between microglia number and DG volume, and regression analysis suggested that microglia number accounted for only a small amount of variation in DG volume, thus the volumetric differences are likely attributable to other sources, for example, disrupted integrity and/or numbers of other types of glia and/or neurons. Astrocytes are functionally linked to microglia (Section 1) and are far more abundant than microglia. Studies are needed to determine whether damage to astrocytes following perturbation of microglia account for DG volume reduction in chronic lead exposure.

Diminished DG volume has implications for learning and memory during development. Just as importantly, the DG is one of the few brain regions in which neurogenesis occurs throughout adulthood (Ming and Song, 2005). Thus, delay of development in DG volume, and/or loss of DG volume during development, would be expected to impact the acquisition of early neurocognitive functions, while also impairing brain resilience in later life. Further studies are needed to examine effects on the aging brain of early chronic exposure to Pb.

4.6. Summary

The findings suggested neuroimmune system disruption, but not chronic neuroinflammation and heightened microglial activation. Furthermore, microglial mean cell body volume differences in animals with lowest vs. higher Pb chronic exposure suggested qualitatively different types of neuroimmune disruption in these groups. Further studies of cytokine levels, in combination with cytokine gene expression, could be useful for confirming these findings. Studies are needed to examine the independent effects on microglia of local Pb concentrations and increased δ-ALA, at lowest and higher chronic and acute doses, and using additional microglial activation markers such as CD45, CD68, and F4/80. Investigating concentrations of Pb in brain and increased brain δ-ALA as distinct neurotoxic triggers may help differentiate their roles in effect pathways. It is also important to examine the effects of early chronic lowest and higher levels of Pb concentrations on progenitor cells. We selected DG as the target structure in these studies because of its critical role in learning and memory, and its role in neurogenesis during adulthood. Additional studies are needed to test for evidence of neuroimmune disruption in other brain regions implicated by results from the child and animal lead exposure literature, including for example, caudate putamen and substantia nigra.

5. Conclusions

Mice chronically exposed to Pb from birth to PND 28, with blood Pb levels from 2.48 to 20.31 μg/dL, had dose-dependent reduction of IL6 gene expression in posterior and anterior brain, significantly less IL6 in posterior brain, dose-dependent reduction in DG microglia mean cell body number, and reduced DG volume. Chronic Pb exposure promoted microglia with broad variability in mean cell body volume, only in animals with blood levels between 2.48 μg/dL and 4.65 μg/dL, and with no increases in inflammatory markers. The findings

lend initial support for neuroimmune system disruption, but not neuroinflammation, as one source of abnormal brain development with chronic developmental exposure to Pb.

Acknowledgments

The authors would like to acknowledge Mari Golub, Environmental Toxicology, UC Davis, for her assistance in the preparation of the final manuscript. The authors would also like to acknowledge Benjamin Valencia for his assistance in the completion of the animal procedures. This research was made possible by grants from the National Institute of Child Health and Human Development (NICHD), National Institutes of Health (R21HD060120, CS, PI); the National Center for Research Resources, a component of the National Institutes of Health (5G12RR008124); the Center for Clinical and Translational Science, The Rockefeller University, New York, New York; the Paso del Norte Health Foundation, El Paso, Texas; the University Research Institute, University of Texas, El Paso; and from the J. Edward and Helen M. C. Stern Professorship in Neuroscience, University of Texas, El Paso (CS). The funders had no role in the design, implementation, data analysis, or manuscript preparation for this study.

Abbreviations

IBA-1	ionized calcium-binding adapter molecule 1
TNF-α	tumor necrosis factor-alpha
IL-1β	interleukin beta 1
IL-6	interleukin 6
IL-10	interleukin 10
IFN-γ	interferon gamma
iNOS	inducible nitric oxide synthase
HO-1	heme oxygenase
ROS	reactive oxygen species
δ-ALA	delta-aminolevulinic acid
DG	dentate gyrus

References

Aloisi F. Immune function of microglia. Glia. 2001; 36:165–179. [PubMed: 11596125]

Azzaoui FZ, Ahami AO, Khadmaoui A. Impact of lead sub-chronic toxicity on recognition memory and motor activity of Wistar rat. Pakistan Journal of Biological Sciences. 2009; 12:173–177. [PubMed: 19579940]

Canfield RL, Henderson CR Jr, Cory-Slechta DA, Cox C, Jusko TA, Lanphear BP. Intellectual impairment in children with blood lead concentrations below 10 microg per deciliter. New England Journal of Medicine. 2003; 348:1517–1526. [PubMed: 12700371]

Chiodo LM, Jacobson SW, Jacobson JL. Neurodevelopmental effects of postnatal lead exposure at very low levels. Neurotoxicology and Teratology. 2004; 26:359–371. [PubMed: 15113598]

Deininger MH, Meyermann R, Schluesener HJ. The allograft inflammatory factor-1 family of proteins. FEBS Letters. 2002; 514:115–121. [PubMed: 11943136]

Dissing-Olesen L, Ladeby R, Nielsen HH, Toft-Hansen H, Dalmau I, Finsen B. Axonal lesion-induced microglial proliferation and microglial cluster formation in the mouse. Neuroscience. 2007; 149:112–122. [PubMed: 17870248]

Dong, HW. The Allen Reference Atlas: A Digital Color Brain Atlas of C57BL/6J Male Mouse. John Wiley & Sons; Hoboken, NJ: 2008.

Emanuelli T, Pagel FW, Prociuncula LO, Souza DO. Effects of 5-aminolevulinic acid on the glutamatergic neurotransmission. Neurochemistry International. 2003; 42:115–121. [PubMed: 12421591]

Espey MG, Chernyshev ON, Reinhard JFJ, Namboodiri MAA, Colton CA. Activated human microglia produce the excitotoxin quinolinic acid. NeuroReport. 1997; 8:431–434. [PubMed: 9080423]

Franklin, K.; Paxinos, G. The Mouse Brain in Stereotaxic Coordinates. Academic Press; San Diego: 1997.

Gaertner, DJ.; Hallman, TM., et al. Anesthesia and analgesia for laboratory rodents. In: Fish, RE.; Brown, MJ.; Danneman, PJ.; Karas, AZ., editors. Anesthesia and analgesia in laboratory animals. Elsevier Press; Philadelphia, PA: 2008. p. 239-297.

Gruol DL, Puro A, Hao C, Blakely P, Janneke E, Vo K. Neuroadaptive changes in cerebellar neurons induced by chronic exposure to IL-6. Journal of Neuroimmunology. 2011; 239:28–36. http://dx.doi.org/10.1016/j.jneuroim.2011.1008.1009 (Epub 2011 September 1013). [PubMed: 21890220]

Gundersen HJ, Jensen EB. The efficiency of systematic sampling in stereology and its prediction. Journal of Microscopy. 1987; 147:229–263. [PubMed: 3430576]

Gundersen HJG, Jensen EBV, Kieu K, Nielsen J. The efficiency of systematic sampling in stereology —reconsidered. Journal of Microscopy. 1999; 193:199–211. [PubMed: 10348656]

Hinkerohe D, Smikalla D, Haghikia A, Heupel K, Haase CG, Dermietzel R, Faustmann PM. Effects of cytokines on microglial phenotypes and astroglial coupling in an inflammatory coculture model. Glia. 2005; 52:85–97. [PubMed: 15920725]

Hsu SM, Raine L, Fanger H. Use of avidin–biotin–peroxidase complex (ABC) in immunoperoxidase techniques: a comparison between ABC and unlabeled antibody (PAP) procedures. Journal of Histochemistry and Cytochemistry. 1981; 29:577–580. [PubMed: 6166661]

Inomata Y, Hirata A, Yonemura N, Koga T, Kido N, Tanihara H. Neuroprotective effects of interleukin-6 on NMDA-induced rat retinal damage. Biochemical and Biophysical Research Communications. 2003; 302:226–232. [PubMed: 12604335]

Ito D, Imai Y, Ohsawa K, Nakajima K, Fukuuchi Y, Kohsaka S. Microglia-specific localisation of a novel calcium binding protein, Iba1. Brain Research. Molecular Brain Research. 1998; 57:1–9. [PubMed: 9630473]

Jessberger S, Clark RE, Broadbent NJ, Clemenson GD, Consiglio A, Lie DC, Squire LR, Gage FH. Dentate gyrus-specific knockdown of adult neurogenesis impairs spatial and object recognition memory in adult rats. Learning & Memory. 2009; 16:147–154. [PubMed: 19181621]

Kasten-Jolly J, Pabello N, Bolivar VJ, Lawrence DA. Developmental lead effects on behavior and brain gene expression in male and female BALB/cAnNTac mice. Neurotoxicology. 2012; 33:1005–1020. http://dx.doi.org/10.1016/j.neuro.2012.1004.1017 (Epub 2012 May 1016). [PubMed: 22609695]

Kaushal V, Koeberle PD, Wang Y, Schlichter LC. The Ca^{2+}-activated K+ channel KCNN4/KCa3.1 contributes to microglia activation and nitric oxide-dependent neurodegeneration. Journal of Neuroscience. 2007; 27:234–244. [PubMed: 17202491]

Kirik O, Sukhorukova E, Korzhevskii D. Calcium-binding protein Iba-1/AIF-1 in rat brain cells. Neuroscience and Behavioral Physiology. 2011; 41:149–152.

Kraft AD, Harry GJ. Features of microglia and neuroinflammation relevant to environmental exposure and neurotoxicity. International Journal of Environmental Research and Public Health. 2011; 8:2980–3018. [PubMed: 21845170]

Lanphear BP, Hornung R, Khoury J, Yolton K, Baghurst P, Bellinger DC, Canfield RL, Dietrich KN, Bornschein R, Greene T, Rothenberg SJ, Needleman HL, Schnaas L, Wasserman G, Graziano J, Roberts R. Low-level environmental lead exposure and children's intellectual function: an international pooled analysis. Environmental Health Perspectives. 2005; 113:894–899. [PubMed: 16002379]

Leasure JL, Giddabasappa A, Chaney S, Johnson JE, Pothakos K, Lau YS, Fox DA. Low-level human equivalent gestational lead exposure produces sex-specific motor and coordination abnormalities and late-onset obesity in year-old mice. Environmental Health Perspectives. 2008; 116:355–361. (Epub 2007 December 2007). [PubMed: 18335103]

Lindahl L, Bird L, Legare M, Mikeska G, Bratton G, Tiffany-Castiglioni E. Differential ability of astroglia and neuronal cells to accumulate lead: dependence on cell type and on degree of differentiation. Toxicological Sciences. 1999; 50:236–243. [PubMed: 10478860]

Livak KJ, Schmittgen TD. Analysis of relative gene expression data using real-time quantitative PCR and the 2(−Delta Delta C(T)) method. Methods. 2001; 25:402–408. [PubMed: 11846609]

Mander PK, Jekabsone A, Brown GC. Microglia proliferation is regulated by hydrogen peroxide from NADPH oxidase. Journal of Immunology. 2006; 176:1046–1052.

Min KJ, Yang MS, Kim SU, Jou I, Joe EH. Astrocytes induce hemeoxygenase-1 expression in microglia: a feasible mechanism for preventing excessive brain inflammation. Journal of Neuroscience. 2006; 26:1880–1887. [PubMed: 16467537]

Minami M, Kuraishi Y, Satoh M. Effects of kainic acid on messenger RNA levels of IL-1 beta, IL-6, TNF alpha and LIF in the rat brain. Biochemical and Biophysical Research Communications. 1991; 176:593–598. [PubMed: 1709015]

Ming G, Song H. Adult neurogenesis in the mammalian central nervous system. Annual Review of Neuroscience. 2005; 28:223–250.

Mohri I, Taniike M, Taniguchi H, Kanekiyo T, Aritake K, Inui T, Fukumoto N, Eguchi N, Kushi A, Sasai H, Kanaoka Y, Ozono K, Narumiya S, Suzuki K, Urade Y. Prostaglandin D2-mediated microglia/astrocyte interaction enhances astrogliosis and demyelination in twitcher. Journal of Neuroscience. 2006; 26:4383–4393. [PubMed: 16624958]

Monif M, Burnstock G, Williams DA. Microglia: proliferation and activation driven by the P2X7 receptor. International Journal of Biochemistry and Cell Biology. 2010; 42:1753–1756. (Epub 2010 July 1753). [PubMed: 20599520]

Mouton PR, Long JM, Lei DL, Howard V, Jucker M, Calhoun ME, Ingram DK. Age and gender effects on microglia and astrocyte numbers in brains of mice. Brain Research. 2002; 956:30–35. [PubMed: 12426043]

Niewoehner B, Single FN, Hvalby O, Jensen V, Meyer zum Alten Borgloh S, Seeburg PH, Rawlins JN, Sprengel R, Bannerman DM. Impaired spatial working memory but spared spatial reference memory following functional loss of NMDA receptors in the dentate gyrus. European Journal of Neuroscience. 2007; 25:837–846. [PubMed: 17313573]

Paolicelli RC, Bolasco G, Pagani F, Maggi L, Scianni M, Panzanelli P, Giustetto M, Ferreira TA, Guiducci E, Dumas L, Ragozzino D, Gross CT. Synaptic pruning by microglia is necessary for normal brain development. Science. 2011; 333:1456–1458. http://dx.doi.org/10.1126/science.1202529 (Epub 1202011 July 1202521). [PubMed: 21778362]

Ransohoff RM, Cardona AE. The myeloid cells of the central nervous system parenchyma. Nature. 2010; 468:253–262. http://dx.doi.org/10.1038/nature09615. [PubMed: 21068834]

Ritter MR, Banin E, Moreno SK, Aguilar E, Dorrell MI, Friedlander M. Myeloid progenitors differentiate into microglia and promote vascular repair in a model of ischemic retinopathy. Journal of Clinical Investigation. 2006; 116:3266–3276. [PubMed: 17111048]

Schafer DP, Lehrman EK, Kautzman AG, Koyama R, Mardinly AR, Yamasaki R, Ransohoff RM, Greenberg ME, Barres BA, Stevens B. Microglia sculpt postnatal neural circuits in an activity and complement-dependent manner. Neuron. 2012; 74:691–705. 610.1016/j.neuron.2012.1003.1026. [PubMed: 22632727]

Schipke, CG.; Boucsein, C.; Ohlemeyer, C.; Kirchhoff, F.; Kettenmann, H. Astrocyte Ca^{2+} waves trigger responses in microglial cells in brain slices. FASEB Journal. 2001. http://dx.doi.org/10.1096/fj.01-0514fje

Schwartz M, Butovsky O, Bruck W, Hanisch UK. Microglial phenotype: is the commitment reversible? Trends in Neurosciences. 2006; 29:68–74. (Epub 2006 January 2006). [PubMed: 16406093]

Sobin C, Parisi N, Schaub T, Gutierrez M, Ortega AX. δ-Aminolevulinic acid dehydratase single nucleotide polymorphism 2 and peptide transporter 2 × 2 haplotype may differentially mediate lead exposure in male children. Archives of Environment Contamination and Toxicology. 2011; 61:521–529. http://dx.doi.org/10.1007/s00244-011-9645-3.

Sola C, Casal C, Tusell JM, Serratosa J. Astrocytes enhance lipopolysaccharide-induced nitric oxide production by microglial cells. European Journal of Neuroscience. 2002; 16:1275–1283. [PubMed: 12405988]

Takeuchi H, Mizuno T, Zhang G, Wang J, Kawanokuchi J, Kuno R, Suzumura A. Neuritic beading induced by activated microglia is an early feature of neuronal dysfunction toward neuronal death

by inhibition of mitochondrial respiration and axonal transport. Journal of Biological Chemistry. 2005; 280:10444–10454. [PubMed: 15640150]

Verderio C, Matteoli M. ATP mediates calcium signaling between astrocytes and microglial cells: modulation by IFN-gamma. Journal of Immunology. 2001; 166:6383–6391.

West MJ, Slomianka L, Gundersen HJ. Unbiased stereological estimation of the total number of neurons in the subdivisions of the rat hippocampus using the optical fractionator. Anatomical Record. 1991; 231:482–497. [PubMed: 1793176]

White LD, Cory-Slechta DA, Gilbert ME, Tiffany-Castiglioni E, Zawia NH, Virgolini M, Rossi-George A, Lasley SM, Qian YC, Basha MR. New and evolving concepts in the neurotoxicology of lead. Toxicology and Applied Pharmacology. 2007; 225:1–27. (Epub 2007 August 2016). [PubMed: 17904601]

Ziv Y, Ron N, Butovsky O, Landa G, Sudai E, Greenberg N, Cohen H, Kipnis J, Schwartz M. Immune cells contribute to the maintenance of neurogenesis and spatial learning abilities in adulthood. Nature Neuroscience. 2006; 9:268–275.

Zonta M, Sebelin A, Gobbo S, Fellin T, Pozzan T, Carmignoto G. Glutamate-mediated cytosolic calcium oscillations regulate a pulsatile prostaglandin release from cultured rat astrocytes. Journal of Physiology. 2003; 553:407–414. [PubMed: 14500777]

HIGHLIGHTS

- Neuroinflammatory markers and microglia were compared in young mice with and without early chronic Pb exposure.
- Mice with Pb levels from 2.66 to 20.31 μg/dL had dose-dependent reduction of cytokine IL6.
- Mice with Pb levels from 2.66 to 20.31 μg/dL had dose-dependent reduction of detectable microglia.
- No evidence of increased neuroinflammation was found.

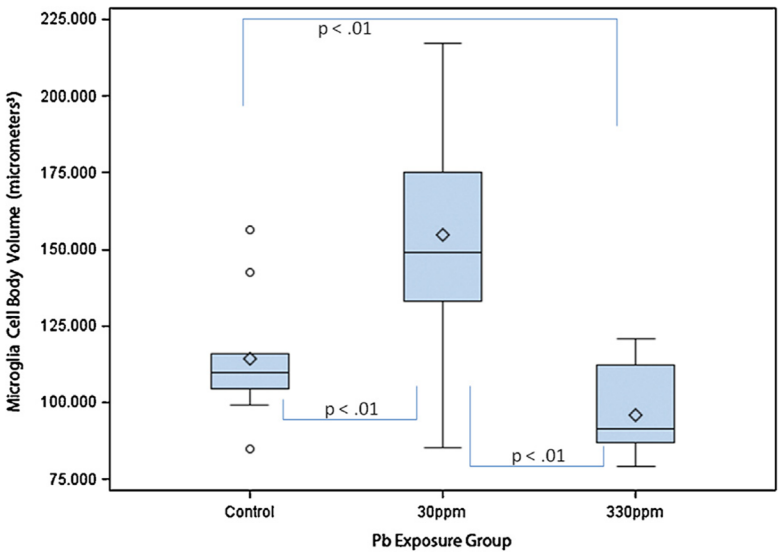

Fig. 1.

Microglia mean cell body volume in μm^3 by exposure group in dentate gyrus. The box plots show the distributions of microglia mean cell body volumes in young C57BL/6J mice exposed to 0 ppm ($n = 10$), 30 ppm ($n = 10$), or 330 ppm ($n = 10$) Pb acetate from birth to PND 28 ($N = 30$). Box plots show the inter-quartile range (25–75th percentile); bars indicate the location of maximum fence values ($\pm 1.5x$ the IQR); central diamond shows the mean; central line shows the median; extreme values are shown with circles. Comparison bars between groups show p values from post hoc tests of marginal ("least square") means. Group difference confidence limits are provided in the text.

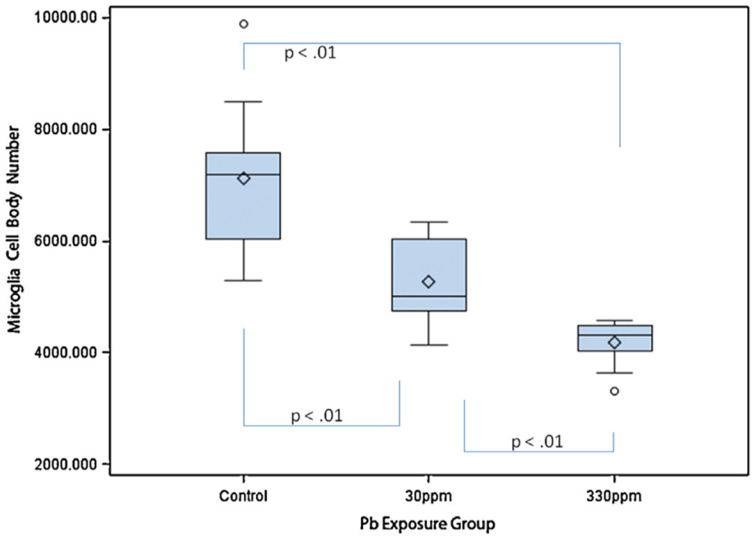

Fig. 2.

Microglia mean cell body number by exposure group in dentate gyrus. The box plots show the distributions of microglia mean cell body numbers by exposure group in young C57BL/6J mice exposed to 0 ppm ($n = 10$), 30 ppm ($n = 10$), or 330 ppm ($n = 10$) Pb acetate from birth to PND 28 ($N = 30$). Box plots show the inter-quartile range (25–75th percentile); bars indicate the location of maximum fence values (±1.5x the IQR); central diamond shows the mean; central line shows the median; extreme values are shown with circles. Comparison bars between groups show p values from post hoc tests of marginal ("least square") means. Group difference confidence limits are provided in the text.

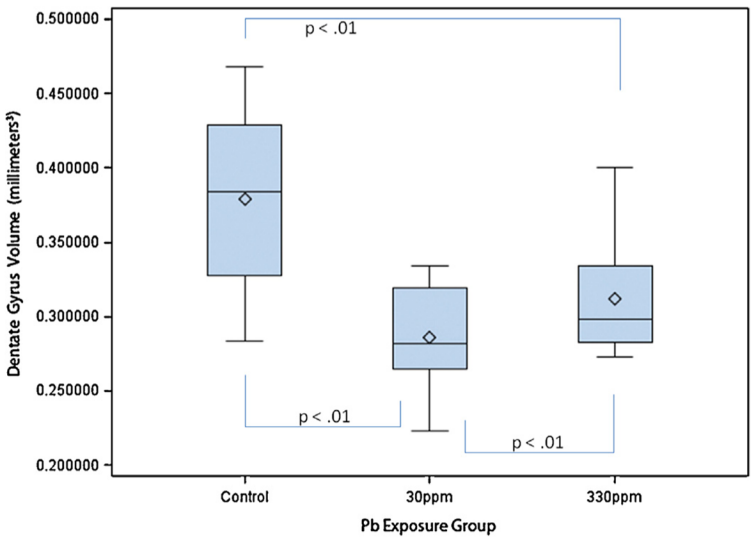

Fig. 3.

Dentate gyri volumes in mm^3 by exposure group. The box plots show the distributions of dentate gyri volumes by exposure group in young C57BL/6J mice exposed to 0 ppm (n = 10), 30 ppm (n = 10), or 330 ppm (n = 10) Pb acetate from birth to PND 28 (N = 30). Box plots show the inter-quartile range (25–75th percentile); bars indicate the location of maximum fence values (±1.5x the IQR); central diamond shows the mean; central line shows the median; extreme values are shown with circles. Comparison bars between groups show p values from post hoc tests of marginal (“least square”) means. Group difference confidence limits are provided in the text.

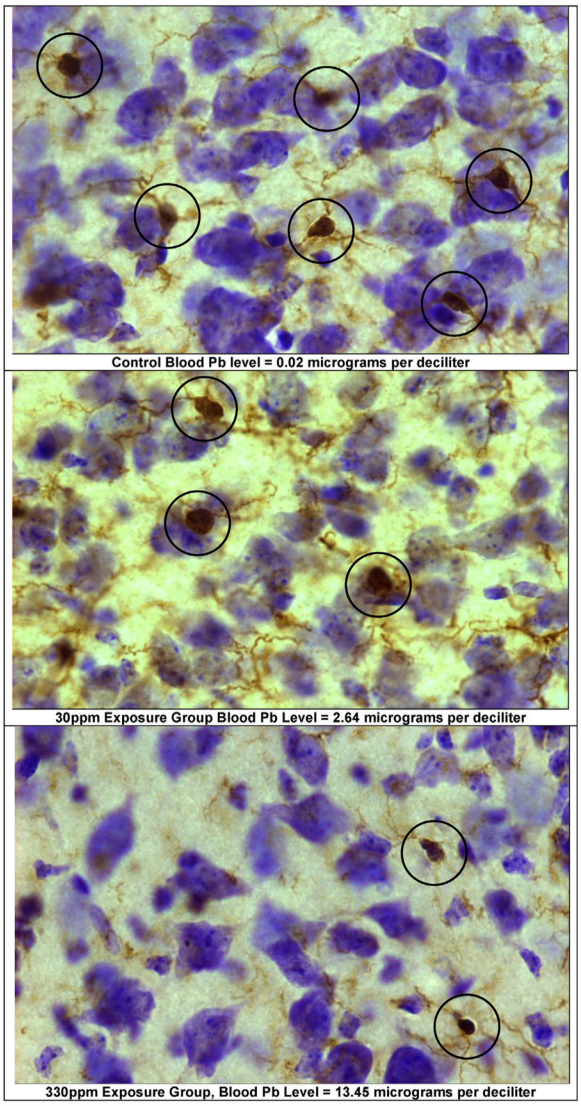

Fig. 4.

Examples of microglia in dentate gyrus. These images show examples of microglia in the dentate gyrus polymorph layer, coronal level 89 captured at 40× (Nikon Plan Oil). The sampling frames are from: (A) a control (0 ppm) animal, blood Pb 0.02 μg/dL; (B) a 30 ppm animal, blood Pb level = 2.64 μg/dL; and (C) a 330 ppm animal, blood Pb level = 13.45 μg/dL. Animals were exposed from birth to PND 28 via dams' drinking water.

Table 1

Mean (SEM) of relative quantification in fold-change of gene expression, in anterior and posterior brain of C57BL/6J mice at PND 28 following chronic Pb exposure.

	Anterior brain (without hippocampus/DG)			Posterior brain (with hippocampus/DG)		
	0 ppm	**30 ppm**	**230 ppm**	**0 ppm**	**30 ppm**	**230 ppm**
TNF	1.05 (0.12)	1.18 (0.30)	1.30 (0.15)	1.00 (0.15)	1.07 (0.20)	1.41 (0.41)
IFN	0.83 (0.05)	1.28 (0.30)	1.11 (0.33)	0.57 (0.05)	1.08 (0.29)	0.87 (0.34).
IL6	2.33 (0.27)	1.72 (0.18)	1.47 (0.29)	1.54 (0.25)	1.23 (0.10)	0.87 (0.20) *
IL10	1.25 (0.14)	1.69 (0.20)	1.27 (0.19)	0.89 (0.11)	1.14 (0.13)	1.20 (0.37)
GRP78	1.61 (0.22)	1.63 (0.23)	1.72 (0.25)	1.54 (0.30)	1.68 (0.19)	1.88 (0.51)
HO-1	1.25 (0.21)	1.14 (0.11)	1.13 (0.14)	1.15 (0.43)	0.85 (0.38)	1.33 (0.46)
iNOS	0.86 (0.07)	1.14 (0.17)	1.06 (0.14)	1.20 (0.28)	0.92 (0.19)	1.42 (0.50)

* ANOVA $p < 0.01$.

Table 2

ANOVA testing for group differences in microglia mean cell body volume and microglia mean cell body number in dentate gyrus, and dentate gyrus volume, in young C57BL/6J mice with and without Pb exposure ($N = 30$).

Source of variation	df	Sum of squares	Mean square	*F*	*p*
Microglia volume (μm^3)					
Group	2	18129.30	9064.65	12.01	<0.01
Error	27	20370.47	754.46		
Microglia number					
Group	2	43,925,346	21,962,673	24.49	<0.01
Error	27	24,216,482	896,907		
Dentate gyrus volume (mm^3)					
Group	2	4.64	2.32	11.50	<0.01
Error	27	5.45	2.02		

Toxicol Lett. Author manuscript; available in PMC 2014 June 20.

Table 3

Coefficient of error (CE) estimates for the measurement of microglia mean cell body volume and microglia mean cell body number in dentate gyrus, and dentate gyrus volume, in young C57BL/6J mice with and without Pb exposure, $N = 30$.

	Microglia mean cell body volume	Microglia mean cell body number	Dentate gyrus volume
0 ppm (controls, $n = 10$)	0.045 (0.006)	0.108 (0.009)	0.091 (0.012)
30 ppm ($n = 10$)	0.036 (0.011)	0.129 (0.016)	0.109 (0.013)
330 ppm ($n = 10$)	0.052 (0.010)	0.134 (0.012)	0.094 (0.020)
All groups	0.044 (0.009)	0.124 (0.012)	0.098 (0.015)